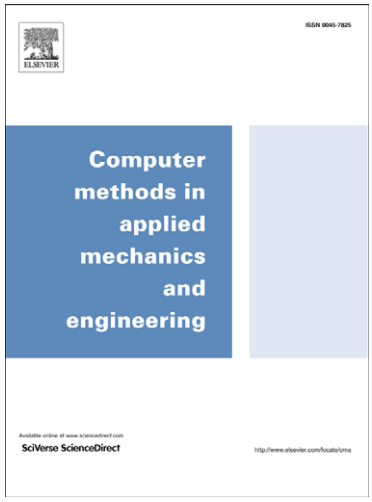

Numerical assessment of stability of interface discontinuous finite element pressure spaces

Fabricio S. Sousa, Roberto F. Ausas, Gustavo C. Buscaglia

PII: S0045-7825(12)00216-2
DOI: http://dx.doi.org/10.1016/j.cma.2012.06.019
Reference: CMA 9756

To appear in: *Comput. Methods Appl. Mech. Engrg.*

Received Date: 7 February 2012
Revised Date: 17 June 2012
Accepted Date: 25 June 2012

Please cite this article as: F.S. Sousa, R.F. Ausas, G.C. Buscaglia, Numerical assessment of stability of interface discontinuous finite element pressure spaces, *Comput. Methods Appl. Mech. Engrg.* (2012), doi: http://dx.doi.org/10.1016/j.cma.2012.06.019

Numerical assessment of stability of interface discontinuous finite element pressure spaces

Fabricio S. Sousa[a,*], Roberto F. Ausas[a], Gustavo C. Buscaglia[a]

[a] *Departamento de Matemática Aplicada e Estatística*
Instituto de Ciências Matemáticas e de Computação, Universidade de São Paulo,
Caixa Postal 668, 13560-970, São Carlos, Brazil

Abstract

The stability of two recently developed pressure spaces has been assessed numerically: The space proposed by Ausas *et al* (Comp. Meth. Appl. Mech. Eng., Vol. 199, 1019-1031, 2010), which is capable of representing discontinuous pressures, and the space proposed by Coppola-Owen and Codina (Int. J. Numer. Meth. Fluids, Vol. 49, 1287-1304, 2005), which can represent discontinuities in pressure gradients. We assess the stability of these spaces by numerically computing the inf–sup constants of several meshes. The inf-sup constant results as the solution of a generalized eigenvalue problems. Both spaces are in this way confirmed to be stable in their original form.

An application of the same numerical assessment tool to the stabilized equal–order P_1/P_1 formulation is then reported. An interesting finding is that the stabilization coefficient can be safely set to zero in an arbitrary band of elements without compromising the formulation's stability. An analogous result is also reported for the mini–element P_1^+/P_1 when the velocity bubbles

*Corresponding author. Phone +55 16 33738173, Fax +55 16 33712238.
Email addresses: f.s.sousa@usp.br (Fabricio S. Sousa), rfausas@gmail.com (Roberto F. Ausas), gustavo.buscaglia@icmc.usp.br (Gustavo C. Buscaglia)

are removed in an arbitrary band of elements.

Keywords: Finite elements, numerical stability, inf-sup condition, eigenvalue problem, discontinuous interpolants

1. Introduction

Accurate numerical simulations of flows dealing with moving interfaces still pose a number of difficulties. In a finite element framework, one of the most pertinent is the representation of discontinuous quantities across the interface, as appearing in free-surface and two-fluid flows, which usually involve discontinuous material properties and/or presence of surface tension effects and singular forces. These discontinuities have to be properly addressed, causing otherwise spurious velocities across the interface and pressure fluctuations. Some considerations were made recently by Ganesan *et al* [1], for problems involving discontinuous pressures, where they end up recommending the use of meshes that follow the interface together with discontinuous pressure interpolants. In fact, that is the only combination of classical finite elements that yields a pressure space that is discontinuous at Γ. However, keeping a mesh of fixed topology aligned with the interface in a dynamic simulation is cumbersome and sometimes impossible. If the alignment is attained by local remeshing, on the other hand, additional burden arises from the interpolation/transfer operators and from the change in the matrix structure. An promising third alternative to maintain alignment has been recently proposed by Rangarajan and Lew [2], but it still lacks sufficient generality (in particular, a three-dimensional version).

Another approach is to consider immersed boundary methods, where the

interface is not aligned with the mesh elements boundaries. In this case, the representation of variables (usually pressure) and their gradient, have to take into account discontinuities induced by the jump in material properties or singular forces. In a finite element framework, this means that interpolation spaces (specially for pressure) must accommodate discontinuities, that are not usually handled by common interpolation spaces.

In the last years, this has been addressed in several ways. Perhaps one of the most popular is the XFEM enrichment technique [3, 4, 5]. This enrichment was employed for the pressure space (see also [6]) to incorporate functions that are discontinuous at the interface Γ, as had also been proposed in [7]. The main drawback of these formulations is the introduction of new unknowns that depend on the location of the interface, thus requiring to rebuild the linear system structure corresponding to each interface location. An additional drawback is that the resulting linear systems are ill-conditioned.

Another type of enrichment was proposed by Coppola-Owen and Codina [8], which is able to represent discontinuous pressure gradients, as happening in two-fluid flows with different densities, under the influence of gravity. Even the most simple stationary flow (lighter fluid above the heavier one, at rest) presents a challenge when discretized by spaces that cannot represent discontinuous pressure gradients. This space is enriched with one pressure degree of freedom inside each finite element crossed by the interface, leading to an enlarged pressure space that will be denoted hereafter by $Q_h^{d\Gamma}$. Contrary to the XFEM case, this extra degree of freedom can be statically condensed before assembling matrices.

In a recent article [9], the authors have introduced a novel pressure space (denoted hereafter by Q_h^Γ) which accommodates discontinuities at a (given) interface Γ. The space Q_h^Γ is nothing but the classical conforming P_1 space, locally modified at those elements of the finite element partition that are cut by the interface. The modification is local, computed element-by-element, and it does not introduce any additional degrees of freedom. This space was implemented for both stable mini-element [10] and stabilized [11, 12] methods. Buscaglia & Agouzal [13] have shown that the interpolation accuracy of Q_h^Γ is $\mathcal{O}(h^{\frac{3}{2}})$ in the $L^2(\Omega)$–norm even if the exact pressure is discontinuous at Γ, but nothing has yet been said about the stability of such modified space.

In fact, to the authors' knowledge, no study about the stability of either $Q_h^{d\Gamma}$ or Q_h^Γ is yet available. Though published results suggest that these spaces produce solutions free of spurious modes, a more rigorous test is needed to properly assess their stability and, thus, their convergence.

For the P_1^+/P_1 mini–element, the famous LBB condition, which guarantees well–posedness and good convergence properties of the discrete formulation is satisfied. The stabilized equal–order P_1/P_1 discretization, though not satisfying the LBB condition, is rendered convergent by introducing into the variational formulation consistent elementwise stabilization (i.e. a stabilization weighted with the residue of the discrete differential operator). In this article we study whether these two discretizations remain stable when the P_1 pressure space is replaced by one of the two aforementioned interface–modified spaces, $Q_h^{d\Gamma}$ or Q_h^Γ.

Direct theoretical proof of stability of the modified pressure spaces is not easy because the space depends on the arbitrary location of the interface.

A proof based on macroelements [14], for example, would require all possible ways in which the interface can cut a macroelement to be worked out explicitly.

Another possibility, which is used in this paper, is the resolution of a suitable eigenvalue problem associated to the discrete inf–sup condition to numerically assess the stability. This can be achieved for any finite element discretization, including both modified spaces considered above. This approach was introduced by Malkus [15], for standard Galerkin formulations, and has been used recently by Huerta et al. [16] to assess meshfree discretizations. Numerical assessments do not constitute rigorous proofs of stability, but are a systematic approach to produce solid evidence of it. By the same token, if the numerical assessment detects a sequence of meshes with eigenvalues tending to zero with refinement, lack of stability can indeed be inferred.

Another positive aspect of the numerical approach to stability is that it is very flexible, it can be applied to any formulation for which the code is available. We take advantage of this to also study a more fundamental question which appeared along the investigation of the modified pressure spaces: Assume that a stable formulation (such as the mini–element one or the stabilized P_1/P_1) is modified by "weakening" its stability in a band of elements (by removing the velocity bubbles or putting to zero the stabilization parameter, respectively, in the elements cut by some interface Γ), *can one expect the resulting formulation to still be stable?* Interestingly, the answer turns out to be affirmative, as is shown (though numerically) in the next sections. This result can be useful when the exact residual at the interface (used in stabilization terms) is not available, as happens when the interface is a capillary

surface discretized using the weak Laplace-Beltrami formula, as in [17, 18]. Unavailability of the interface residual can also happen when very complex interfaces are treated by multi-scale techniques (with a separate Molecular Dynamics code, for example).

The article is organized as follows: In section 2 we present the exact and discrete variational formulations for the Stokes problem. In section 3, we write the eigenvalue problem that yields the stability constant of Galerkin formulations, as originally introduced by Malkus [15]. Further, we generalize this eigenproblem so as to compute the stability constant of stabilized discretizations. Section 4 recalls the description of the two pressure finite element spaces under scrutiny. The numerical stability assessment itself is presented in section 5, and finally, conclusions are drawn in section 6.

2. Mathematical setting

The numerical stability study is restricted to the Stokes problem

$$
\begin{aligned}
-\nabla\cdot\left[\mu(\nabla u+\nabla u^T)\right]+\nabla p &= F_\Gamma+\rho\, g \quad \text{in } \Omega && (1)\\
\nabla\cdot u &= 0 \quad \text{in } \Omega && (2)\\
u &= 0 \quad \text{on } \partial\Omega && (3)
\end{aligned}
$$

where $\Omega\subset\mathbb{R}^d$ and Γ is a surface (curve in 2D) that divides Ω into two subdomains Ω_1 and Ω_2. Pressure discontinuities arise from a surface force applied directly on Γ. A force acting on the surface Γ can be modeled by $F_\Gamma = f\,\delta_\Gamma\,\mathbf{n}$, with f a given function, δ_Γ the Dirac delta distribution on the surface Γ, and $\mathbf{n}$ its normal. The singular force F_Γ acts in fact as a jump

condition on the normal stress across Γ, namely,

$$\left[\!\left[-p + 2\mu\frac{\partial u_n}{\partial n}\right]\!\right] = f. \tag{4}$$

where $[\![g]\!]$ stands for the jump across Γ of a generic quantity g.

Density jumps lead to kinks in the pressure field at the interface. This is easily seen in the prototypical example of two fluids with different densities at rest, one on top of the other. The hydrostatic pressure gradient is discontinuous at the interface. The velocity field being identically zero, the pressure gradient is $\nabla p = \rho\, g$, therefore giving

$$[\![\nabla p]\!] = [\![\rho\, g]\!] = [\![\rho]\!]\, g = (\rho_1 - \rho_2)\, g\ . \tag{5}$$

2.1. Exact variational formulation

Denoting by $V = [H_0^1(\Omega)]^d$, $Q = L^2(\Omega)/\mathbb{R}$ and $W = V \times Q$, the variational formulation that corresponds to (1)-(3) reads: "Find $(u, p) \in W$ such that

$$\int_\Omega \left[\mu(\nabla u + \nabla u^T) : \nabla v - p\ \nabla\cdot v + q\ \nabla\cdot u\right]\ d\Omega = \int_\Gamma f\ \mathbf{n}\cdot v\, d\Gamma + \int_\Omega \rho g\cdot v\, d\Omega \tag{6}$$

for all $(v, q) \in W$". In (6) the symbol ":" stands for the double contraction of rank–two tensors. The bilinear and linear forms associated to the variational formulation are denoted by $B(\cdot,\cdot)$ and $L(\cdot)$, so that (6) can be rewritten as

$$B((u, p), (v, q)) = L((v, q)). \tag{7}$$

Under reasonable regularity assumptions on Γ and f the linear functional L is bounded. Assuming also appropriate conditions on Ω, and denoting by $\mathbf{u}$ and $\mathbf{v}$ the pairs (u, p) and (v, q) respectively, problem (6) is well–posed since the following known properties hold for B:

$$|B(\mathbf{u}, \mathbf{v})| \le \alpha \|\mathbf{u}\|_W \|\mathbf{v}\|_W \tag{8}$$

$$\inf_{\mathbf{v}\in W}\sup_{\mathbf{u}\in W}\frac{B(\mathbf{u},\mathbf{v})}{\|\mathbf{u}\|_W\,\|\mathbf{v}\|_W}>0 \tag{9}$$

with α a constant and $\|\cdot\|_W$ the induced norm on W which for a function $\mathbf{u}=(u,p)\in W$ is given by

$$\|\mathbf{u}\|_W^2=\|(u,p)\|_W^2=\|u\|_V^2+\frac{1}{\mu}\|p\|_Q^2 \tag{10}$$

Also, the next form of problem (6) is useful in what follows

$$a(u,v) \;-\; b(p,v) \;=\; l(v) \qquad \forall v\in V \tag{11}$$

$$b(q,u) \;=\; 0 \qquad \forall q\in Q \tag{12}$$

where the bilinear forms $a(\cdot,\cdot)$ and $b(\cdot,\cdot)$ and the linear form $l(\cdot)$ are respectively given by

$$a(u,v) \;=\; \int_\Omega \mu(\nabla u+\nabla u^T):\nabla v\,d\Omega \quad \forall v\in V \tag{13}$$

$$b(p,v) \;=\; \int_\Omega p\;\nabla\cdot v\,d\Omega \quad \forall q\in Q \tag{14}$$

$$l(v) \;=\; \int_\Gamma f\;\mathbf{n}\cdot v\,d\Gamma+\int_\Omega \rho g\cdot v\,d\Omega \quad \forall v\in V \tag{15}$$

Now, based on (13), we introduce the next equivalent norm on V to be used later on

$$\|v\|_V=\sqrt{a(v,v)} \quad \forall\; v\in V\;. \tag{16}$$

2.2. Discrete variational formulation

This part introduces the discrete countepart of problem (7) or of its equivalent form (11)–(12). The discrete variational formulations for both the mini–element discretization and the stabilized discretization are detailed.

2.2.1. Galerkin mini–element formulation

In the Galerkin formulation, the exact variational problem is restricted to the space $W_h = V_h \times Q_h$, where $V_h \subset V$ and $Q_h \subset Q$ are the approximation spaces for velocity and pressure respectively. The discrete formulation thus reads "Find $(u_h, p_h) \in V_h \times Q_h$ such that

$$B((u_h, p_h), (v_h, q_h)) = l(v_h) \tag{17}$$

for all $(v_h, q_h) \in V_h \times Q_h$". The mesh parameter h tends to zero as the mesh is refined.

The pressure and velocity spaces that correspond to the so-called mini-element [10] are, for a finite element mesh $\mathcal{T}_h$, given by:

$$Q_h = Q_h^1 := \{q_h \in Q \cap \mathcal{C}^0(\Omega),\ q_h|_K \in P_1(K),\ \forall\, K \in \mathcal{T}_h\} \tag{18}$$

$$V_h = V_h^{\text{mini}} := \{v_h \in V,\ v_h|_K \in (P_1(K) \oplus \text{span}(b_K))^d,\ \forall\, K \in \mathcal{T}_h\} \tag{19}$$

where b_K is the bubble function that vanishes on the boundary of K. Note that the pressure space is nothing but the usual continuous P_1 space, while the space for each velocity component has been enriched by the bubble functions.

The matrix form of problem (17) is also useful for the rest of the article. Let $\{N_a\}_{1\le a\le n_u}$ be a basis for the discrete space V_h (of dimension n_u) and $\{M_a\}_{1\le a\le n_p}$ be a basis for the discrete space Q_h (of dimension n_p) and assume the following expansions for u_h and p_h

$$u_h = \sum_{a=1}^{n_u} u_a N_a, \qquad p_h = \sum_{a=1}^{n_p} p_a M_a \tag{20}$$

Now, denoting by $\mathbf{u} = (\mathsf{U}, \mathsf{P})^T = (u_1, \ldots, u_{n_u}, p_1, \ldots, p_{n_p})^T$, the global col-

umn vector of nodal unknowns, problem (17) can be rewritten as

$$\begin{bmatrix} \mathbf{A} & \mathbf{B} \\ \mathbf{B}^T & \mathbf{0} \end{bmatrix} \begin{bmatrix} \mathsf{U} \\ \mathsf{P} \end{bmatrix} = \begin{bmatrix} \mathsf{F} \\ 0 \end{bmatrix} \tag{21}$$

where $\mathsf{F}_a = l(N_a)$, $\mathbf{A} \in \mathbb{R}^{n_u \times n_u}$ and $\mathbf{B} \in \mathbb{R}^{n_u \times n_p}$. The element ab of these matrices is respectively given by

$$\mathbf{A}_{ab} = a(N_a, N_b) \tag{22}$$

$$\mathbf{B}_{ab} = -b(M_a, N_b) \tag{23}$$

2.2.2. Stabilized formulation

We are also interested in considering stabilized finite element formulations that do not satisfy the Ladyzhenskaya-Babuška-Brezzi condition (further details in section 3), but are rendered convergent by means of stabilization techniques [11, 12]. This is the case of the equal-order P_1/P_1 formulation in which the discrete spaces are

$$Q_h = Q_h^1 \quad \text{(as before)} \tag{24}$$

$$V_h = V_h^1 := \{v_h \in V,\ v_h|_K \in P_1(K)^d,\ \forall K \in \mathcal{T}_h\} \tag{25}$$

and the formulation reads: "Find $(u_h, p_h) \in V_h \times Q_h$ such that

$$B_S((u_h, p_h), (v_h, q_h)) = l(v_h) \tag{26}$$

for all $(v_h, q_h) \in V_h \times Q_h$". The bilinear form B_S that incorporates the stabilization is given by

$$B_S((u_h, p_h), (v_h, q_h)) = a(u_h, v_h) - b(p_h, v_h) + b(q_h, u_h) + \sum_{K \in \mathcal{T}_h} \tau_K \left\{ \int_K \mathcal{R}(u_h, p_h) \cdot \nabla q_h \, dK + \int_{\Gamma \cap K} \mathcal{R}_\Gamma [\![q_h]\!] \, d\Gamma \right\} \tag{27}$$

with the residuals $\mathcal{R}$ and $\mathcal{R}_\Gamma$ defined as

$$\mathcal{R}(u_h, p_h) = -\nabla \cdot \left[\mu(\nabla u_h + \nabla u_h^T)\right] + \nabla p_h - \rho g \tag{28}$$

and

$$\mathcal{R}_\Gamma(u_h, p_h) = \left(\left[\!\left[-p_h \mathbb{I} + \mu(\nabla u_h + \nabla u_h^T)\right]\!\right] \cdot \mathbf{n}\right) \cdot \mathbf{n} - f. \tag{29}$$

Note that in our case (constant viscosity, P_1 elements) the first term of (28) is identically zero and that, if the pressure space is continuous across Γ, the jump $[\![q_h]\!]$ multiplying the interface residual $\mathcal{R}_\Gamma$ in (27) is identically zero.

The corresponding problem in matrix form reads

$$\begin{bmatrix} \mathbf{A} & \mathbf{B} \\ \mathbf{B}^T & \mathbf{C} \end{bmatrix} \begin{bmatrix} \mathsf{U} \\ \mathsf{P} \end{bmatrix} = \begin{bmatrix} \mathsf{F} \\ \mathsf{G} \end{bmatrix} \tag{30}$$

where the matrix $\mathbf{C}$ which incorporates the stabilization is defined as

$$\mathbf{C}_{ab} = \sum_{K \in \mathcal{T}_h} \tau_K (\nabla M_a, \nabla M_b) \ . \tag{31}$$

Finally, as explained in [19], for a function $\mathbf{u}_h \in W_h$, in this case, the following norm on W is used

$$\|\mathbf{u}_h\|_W^2 = \|(u_h, p_h)\|_W^2 = \|u_h\|_V^2 + \frac{1}{\mu}\|p_h\|_Q^2 + \sum_{K \in \mathcal{T}_h} \tau_K \|\nabla p_h\|_Q^2 \ . \tag{32}$$

3. Stability conditions

For a Galerkin finite element formulation to be well–posed and convergent it is sufficient that the celebrated Ladyzhenskaya-Babuška-Brezzi stability condition [20, 21] be satisfied:

$$\inf_{q_h \in Q_h} \sup_{v_h \in V_h} \frac{b(q_h, v_h)}{\|q_h\|_Q \ \|v_h\|_V} \geq \gamma_0 > 0 \tag{33}$$

with γ_0 a mesh-independent constant. This certanly holds for the case of the mini–element discretization, but not for equal–order ones, which require stabilization. An way to investigate the stability of a finite element discretization, not necessarily of the Galerkin type, is to compute the following inf–sup constant:

$$\beta_h \doteq \inf_{(v_h,q_h)\in W_h} \sup_{(u_h,p_h)\in W_h} \frac{\mathcal{B}((u_h,p_h),(v_h,q_h))}{\|(u_h,p_h)\|_W \, \|(v_h,q_h)\|_W} \tag{34}$$

where the bilinear form $\mathcal{B}(\cdot,\cdot)$ can be either $B(\cdot,\cdot)$ defined in (6) for the mini–element discretization or $B_S(\cdot,\cdot)$ defined in (27) for the stabilized formulation. The sufficient stability condition is now that there exists $\beta_0 > 0$, independent of the mesh, such that

$$\beta_h \geq \beta_0 > 0 \tag{35}$$

as the mesh is refined ($h \to 0$). The relevance of the inf–sup condition regarding the convergence of the finite element discretizations follows from the next inequality that can be easily proved

$$\|\mathbf{u} - \mathbf{u}_h\|_W \leq \left(1 + \frac{\alpha}{\beta_0}\right) \inf_{\mathbf{v}_h \in W_h} \|\mathbf{u} - \mathbf{v}_h\|_W \tag{36}$$

where $\mathbf{u} = (u, p)$, $\mathbf{u}_h = (u_h, p_h)$ and α is the constant (independent of h) that appears in the continuity condition for the bilinear form (8).

3.1. The inf–sup *eigenvalue problem*

For a given mesh, the inf–sup constant β_h defined in (34) can be computed as follows. Considering (10) and (16), the norm on W in matrix form reads

$$\|(u_h,p_h)\|_W^2 = \mathsf{U}^T \mathbf{A} \mathsf{U} + \mathsf{P}^T \mathbf{Q} \mathsf{P} \tag{37}$$

where the pressure mass matrix $\mathbf{Q} \in \mathbb{R}^{n_p \times n_p}$ for the case of the mini–element discretization is defined as

$$\mathbf{Q}_{ab} = \frac{1}{\mu}(M_a, M_b) \tag{38}$$

The norm (32) associated to the stabilized discretization, on the other hand, is written in matrix form as

$$\|(u_h, p_h)\|_W^2 = \mathsf{U}^T \mathbf{A} \mathsf{U} + \mathsf{P}^T \mathbf{Q} \mathsf{P} + \mathsf{P}^T \mathbf{E} \mathsf{P} \tag{39}$$

with matrix $\mathbf{C}$ defined in (31). By further defining the matrices $\mathbf{N}, \mathbf{K} \in \mathbb{R}^{(n_u+n_p)\times(n_u+n_p)}$ as

$$\mathbf{N} = \begin{bmatrix} \mathbf{A} & \mathbf{0} \\ \mathbf{0} & \mathbf{Q}+\mathbf{E} \end{bmatrix} \qquad \mathbf{K} = \begin{bmatrix} \mathbf{A} & \mathbf{B} \\ \mathbf{B}^T & \mathbf{E} \end{bmatrix} \tag{40}$$

where $\mathbf{E} \in \mathbb{R}^{n_p \times n_p}$ is identically $\mathbf{0}$ for the Galerkin formulation while for the stabilized one it corresponds to the matrix $\mathbf{C}$. We can now write the norm on W as

$$\|(u_h, p_h)\|_W^2 = \mathbf{u}^T \mathbf{N} \mathbf{u} \ , \tag{41}$$

where $\mathbf{u} = (\mathsf{U}, \mathsf{P})^T$, and the quotient in (34) as

$$R(\mathbf{u}, \mathbf{v}) = \frac{\mathbf{u}^T \mathbf{K} \mathbf{v}}{(\mathbf{u}^T \mathbf{N} \mathbf{u})^{\frac{1}{2}} (\mathbf{v}^T \mathbf{N} \mathbf{v})^{\frac{1}{2}}} \tag{42}$$

It can then be shown that β_h, which is the inf–sup value of (42), is the smallest (in magnitude) eigenvalue of the following generalized eigenvalue problem

$$\mathbf{K}\mathbf{u} = \lambda \mathbf{N}\mathbf{u} \tag{43}$$

Also the number of zero eigenvalues (if any) indicates the number of spurious modes. Although this is presented and well discussed by Malkus [15] for non-stabilized formulations, we could not find any similar work for stabilized finite

element discretizations. The needed modification, however, simply consists of adding the matrix block $\mathbf{E}$ as written in Eq. (40).

Remark. Observe that the eigenvalues for this problem are in $\{\mathbb{R} \setminus (0,1)\}$. To see this, eliminate P from the system (43), i.e.,

$$\mathbf{B}\mathbf{Q}^{-1}\mathbf{B}^T\mathsf{U} = (\lambda^2 - \lambda)\mathbf{A}\mathsf{U} \tag{44}$$

After premultiplication of both sides by U^T one obtains

$$(\mathbf{B}^T\mathsf{U})^T\mathbf{Q}^{-1}(\mathbf{B}^T\mathsf{U}) = (\lambda^2 - \lambda)(\mathsf{U}^T\mathbf{A}\mathsf{U}) \tag{45}$$

Now, noting that the left hand side and the factor $\mathsf{U}^T\mathbf{A}\mathsf{U}$ are both positive, it follows that $\lambda^2 - \lambda > 0$ and thus $\lambda \in \{\mathbb{R} \setminus (0,1)\}$.

4. Description of modified pressure spaces

In this section, we briefly recall the definition of two different pressure spaces, one capable of representing discontinuous pressures [9], that is suitable for surface tension flows, and another that can capture discontinuities in the pressure gradient [8], suitable for two-fluid flows with different densities in the presence of gravity. We evaluate the convergence of these two pressure spaces, studying the associated eigenvalue inf–sup problem, in the next section.

4.1. Discontinuous pressure space

The underlying idea behind the discontinuous pressure space presented in [9] is to locally modify the classical conforming P_1 space at those elements of $\mathcal{T}_h$ that are cut by the interface so as to admit discontinuities at Γ. In the

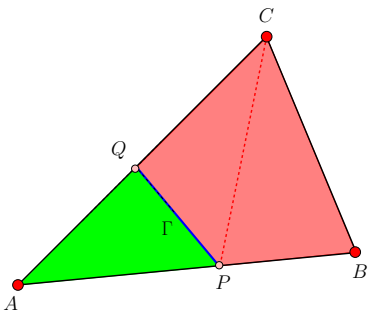

Figure 1: Partition of a single finite element into subelements following the interface PQ.

rest of the mesh the standard P_1 interpolants are chosen. We denote this new pressure space by Q_h^Γ. Here, for the sake of brevity we discuss how to construct Q_h^Γ for the elements crossed by the interface, but restrict ourselves to the two–dimensional case. The complete description and details, for the three–dimensional case, even for cases in which the interface Γ has and end point or a boundary inside a given element, can be found in [9, 22].

Consider the triangle ABC, which is cut by Γ into subtriangle APQ and subquadrilateral $BCQP$ (see Fig. 1). We assume for simplicity that, locally, Γ is approximated by linear segments Let p_A, p_B, p_C denote the nodal values of the discrete pressure p_h, to be interpolated in the triangle ABC.

Let us arbitrarily denote the triangle APQ the "green" side of Γ and quadrilateral $BCQP$ the "red" side. For the approximation to be discontinuous, the function p_h on the green side needs to be solely determined by the only green node, i.e., A. Similarly, p_h on the red side must depend on just p_B and p_C. To accomplish this, we simply "carry" the value at each node towards the intersection of any edge emanating from it with the interface.

In this way, on the green side of Γ, the values at P and Q will be p_A, and

thus p_h will be constant:

$$p_h|_{APQ} = p_A$$

On the red side, the value at P will be p_B and the value at Q will be p_C. One can here choose either to adopt a Q_1 interpolation in $BCQP$ from these nodal values, or subdivide the quadrilateral into two triangles, BCP and CQP. In any case, since the nodal values are given, the interpolation is immediate. For the red triangle CQP, for example, p_h will be the linear function that takes the value p_C at vertex C, the value p_C at vertex Q, and the value p_B at vertex P. Notice that this interpolation leads to p_h being discontinuous *only at* Γ, since the function p_h restricted to any edge of the triangle is uniquely determined by the values at the nodes lying at the endpoints of that edge.

The basis functions N_A, N_B and N_C (illustrated in Fig. 2) are defined to be piecewise affine inside each of these subtriangles. It only remains to define their values at the vertices of the subtriangles, i.e., at the points A, B, C, P and Q. However, since they are discontinuous at Γ, two values are given at points P and Q. The values on the green side will be assigned a "plus" sign, while those on the red side a "minus" sign. The values at the vertices are:

$$N_A(\,A\,) = 1 \quad N_B(\,A\,) = 0 \quad N_C(\,A\,) = 0 \tag{46}$$

$$N_A(\,B\,) = 0 \quad N_B(\,B\,) = 1 \quad N_C(\,B\,) = 0 \tag{47}$$

$$N_A(\,C\,) = 0 \quad N_B(\,C\,) = 0 \quad N_C(\,C\,) = 1 \tag{48}$$

$$N_A(P^+) = 1 \quad N_B(P^+) = 0 \quad N_C(P^+) = 0 \tag{49}$$

$$N_A(P^-) = 0 \quad N_B(P^-) = 1 \quad N_C(P^-) = 0 \tag{50}$$

$$N_A(Q^+) = 1 \quad N_B(Q^+) = 0 \quad N_C(Q^+) = 0 \tag{51}$$

$$N_A(Q^-) = 0 \quad N_B(Q^-) = 0 \quad N_C(Q^-) = 1 \tag{52}$$

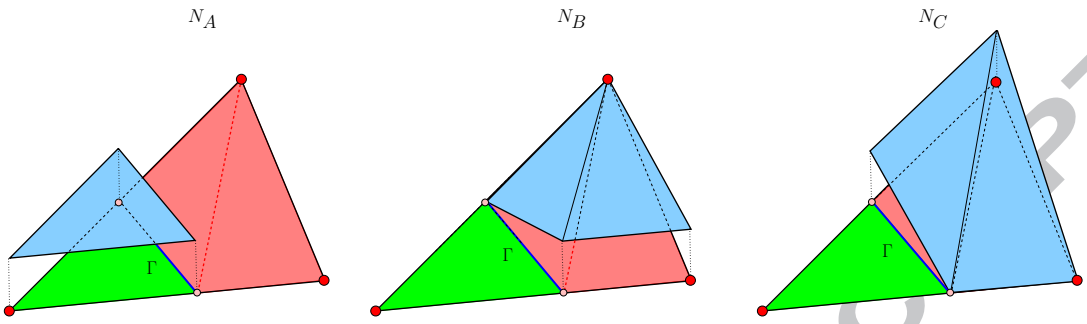

Figure 2: Basis functions for the new finite element space inside an element crossed by the interface: (a) N_A, (b) N_B and (c) N_C.

The interpolation properties of the new space are shown numerically in [9] by means of several numerical tests, including problems with imposed singular forces and problems with surface tension effects, both in 2D and 3D. Also a theoretical proof of convergence for the interpolation has been presented in [13]. Briefly, the interpolation accuracy of the proposed space is $\mathcal{O}(h^{\frac{3}{2}})$ in the $L^2(\Omega)$–norm, which is suboptimal for piecewise linear elements. However, Q_h^Γ does not limit the accuracy of a (Navier–) Stokes calculation, neither in equal–order velocity–pressure approximations nor in the mini–element approximation. In fact, in both approximations the overall accuracy is limited by the $H^1(\Omega)$–accuracy of the velocity space, since the error estimate is

$$\begin{aligned} \|u-u_h\|_V + \|p-p_h\|_Q &\leq C\left(\inf_{w_h\in V_h}\|u-w_h\|_V + \inf_{r_h\in Q_h}\|p-r_h\|_Q\right) \\ &\leq C\left(c_1\,h\,|u|_{H^2(\Omega)} + c_2\,h^{\frac{3}{2}}\,|p|_{H^2(\Omega\setminus\Gamma)}\right) \\ &= \mathcal{O}(h) \end{aligned} \tag{53}$$

where C, c_1 and c_2 do not depend on the mesh size h.

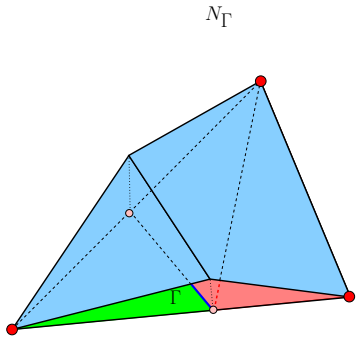

Figure 3: Enrichment function for the discontinuous pressure gradient space $Q_h^{d\Gamma}$.

4.2. Enriched discontinuous pressure gradient space

The idea of this pressure space, which is presented in detail in [8], is to enrich the P_1 space with one degree of freedom per element of $\mathcal{T}_h$ cut by the interface. The enrichment function is constructed to be continuous across Γ, but with gradient being constant (and different) on each side of the interface. Thus this pressure space, that we denote by $Q_h^{d\Gamma}$, is composed of standard P_1 interpolation plus the additional shape function for elements crossed by the interface, and standard P_1 interpolation for elements away from the interface. One advantage of such space is that the added degrees of freedom can be statically condensed before matrix assembly, unlike in other approaches like XFEM.

Consider the same triangle ABC cut by Γ in a straight line segment joining points P and Q as in Fig. 1. This function can be easily defined with the help of a level set function Φ_h (whose zero set is Γ) linearly interpolated on ABC and with the usual P_1 functions N_J, $J = 1, \ldots, n_p$ ($n_p = 3$ in 2D and $n_p = 4$ in 3D). The enrichment function (see Fig. 3) is then defined as

$$N_\Gamma(x) = \frac{1}{2}\left(-|\Phi_h(x)| + \sum_{J=1}^{n_p} |\Phi_h(x_J)| N_J(x)\right), \tag{54}$$

As stated in [8], as the pressure is enriched, this could lead to an unstable velocity-pressure pair. Even using a stabilized formulation (as the authors did), no stability analysis is discussed in [8]. They did not encounter any stability misbehavior, but it is still unclear how this enrichment affects the overall convergence of this finite element discretization.

Remark. For both spaces described here the quadrature rules should also be adapted to accommodate the interface Γ. This can be easily done by dividing the element (triangle or tetrahedra) in subelements, according to Γ, and applying a standard quadrature rule to the subelements.

5. Numerical stability analysis

In this section, we analyze the stability of the pressure spaces described in section 4, by solving the generalized eigenvalue problem (43). To accomplish that, we use the SLEPc routines (Scalable Library for Eigenvalue Problem Computations, [23]) with their default solver based on a Krylov-Schur method. The homogeneous Dirichlet boundary conditions are dealt by means of replacing the corresponding rows and columns in the system matrices with vectors containing zero entries at all positions except at the one corresponding to the diagonal where an arbitrary value of 1000 and 1 are placed on the left and right hand side matrices respectively. In this way we are able to shift these eigenvalues (all equal to 1000) that are unimportant to us.

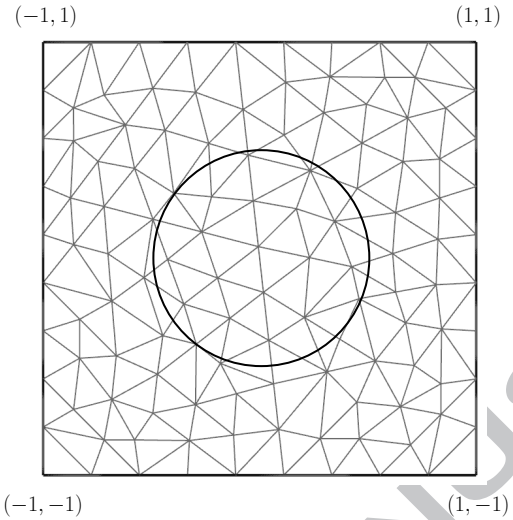

Figure 4: First mesh of the sequence used to numerically asses the stability of the finite element discretizations with the pressure spaces Q_h^{Γ} and $Q_h^{d\Gamma}$.

We consider two different computational domains. The first one is set to be the two-dimensional square $\Omega = [-1, 1]^2$ which is discretized with an unstructured mesh consisting of 208 triangular elements (shown in figure 4) which corresponds to a mesh size of $h_0 = 0.2$. A sequence of meshes is built by successively dividing each of the triangles of the previous mesh into four equal triangles leading to meshes with $h_1 = h_0/2$, $h_2 = h_0/4$ and so forth, until the finest mesh with $h_5 = 6.25 \times 10^{-3}$ (with 212992 elements). The second one is set to be the three-dimensional cube $\Omega = [-1, 1]^3$, discretized by a mesh of 4392 tetrahedra, with mesh size $h_0 = 0.2$. Two additional finer meshes are built (not by direct subdivision of all elements), with mesh sizes $h_1 = 0.1$ and $h_2 = 0.05$, with 35136 and 281088 tetrahedra, respectively.

In the numerical implementation, the interface Γ is in fact not considered exactly but approximated as follows: Let Φ be a continuous scalar function

whose zero level set represents the exact interface Γ, i.e.

$$\Gamma = \left\{ \boldsymbol{x} \in \mathbb{R}^d,\ \Phi(\boldsymbol{x}) = 0 \right\}. \tag{55}$$

The function Φ is then linearly interpolated on each element $K \in \mathcal{T}_h$, and the zero level set of the resulting Φ_h is then used instead of Γ in all the numerical expressions. In the initial tests the exact Γ consists of a circle in 2D and of a sphere in 3D, of radius 0.5, centered at the origin. Later on other interface shapes will appear. The reader should note that, since we are not solving the flow equations but the inf-sup eigenvalue problem, there is no right-hand-side coming from the interface. Thus, the only effect of an element K being crossed by Γ is to switch the pressure interpolants inside K from P_1 to the discontinuous space Q_h^Γ or the enriched space $Q_h^{d\Gamma}$.

To gain further insight on the effects of modifying the formulation on the band of elements crossed by Γ, we will consider two variants for the choice of the stabilization parameter. The **standard** version of stabilization is defined by taking

$$\tau_K = \frac{h_K^2}{4\mu}, \tag{56}$$

where h_K is the element size, for all elements K in $\mathcal{T}_h$. The **weakened** version, instead, takes

$$\tau_K = \begin{cases} 0 & \text{if } K \text{ is cut by } \Gamma \\ h_K^2/4\mu & \text{otherwise} \end{cases} \tag{57}$$

It removes all stabilization terms in the band of elements cut by Γ, which will be denoted hereafter $\mathcal{A}_h$.

By analogy, standard and weakened versions of the mini-element formulation are defined as follows: In the **standard** version, the velocity space is

V_h^{mini} as usual, whichever the pressure space being analyzed. In the **weakened** version, the velocity space is taken as

$$V_h^{\text{mini},0} := \{v_h \in V_h^{\text{mini}},\ v_h|_K \in P_1(K)^d,\ \forall\, K \in \mathcal{A}_h\}\ , \tag{58}$$

In other words, the velocity bubble functions have been removed in the elements cut by Γ. In *any* version of the mini-element, as usual, the Galerkin bilinear form is adopted.

We are now in a position to introduce the four cases that will be reported to some extent here, since not all combinations are worth discussing. These cases, defined by the pressure-velocity combination of spaces and by the formulation adopted, are:

- **Case A:** Q_h^Γ–V_h^1, with *weakened* stabilization;
- **Case B:** Q_h^Γ–$V_h^{\text{mini},0}$ (i.e., *weakened mini*);
- **Case C:** $Q_h^{d\Gamma}$–V_h^1 with *standard* stabilization;
- **Case D:** $Q_h^{d\Gamma}$–V_h^1 with *weakened* stabilization;

5.1. Stability assessment of Q_h^Γ (Cases A and B)

The inf–sup eigenproblem (43) is solved in order to obtain the four smallest (in magnitude) eigenvalues both in 2D and 3D. Tables 1 and 2 display the numerically computed eigenvalues for the two-dimensional domain for case A and case B, respectively. The negative signs in all the numbers have been omitted for clarity.

Remembering that the smallest eigenvalue $|\lambda_1|$ of the generalized problem (43) is the inf–sup constant β_h, an eigenvalue approaching zero as the mesh is

Table 1: First four eigenvalues obtained for case A, in 2D.

h	λ_1	λ_2	λ_3	λ_4
h_0	0.18385	0.18655	0.18792	0.22705
$h_0/2$	0.17048	0.17193	0.17242	0.19374
$h_0/4$	0.16205	0.16305	0.16312	0.17673
$h_0/8$	0.15608	0.15678	0.15679	0.16580
$h_0/16$	0.15190	0.15241	0.15241	0.15868
$h_0/32$	0.14890	0.14928	0.14928	0.15384

Table 2: First four eigenvalues obtained for case B, in 2D.

h	λ_1	λ_2	λ_3	λ_4
h_0	0.07619	0.07638	0.07644	0.07692
$h_0/2$	0.07837	0.07861	0.07863	0.07963
$h_0/4$	0.07813	0.07815	0.07816	0.07851
$h_0/8$	0.07810	0.07811	0.07811	0.07823
$h_0/16$	0.07809	0.07809	0.07809	0.07814
$h_0/32$	0.07811	0.07818	0.07819	0.07826

refined would indicate lack of stability. Table 1 shows that $|\lambda_1|$ does not tend to zero in Case A, but rather to about 0.149. Note that after six refinements the eigenvalue has changed very little (less than 20%), making it very unlikely that with further refinements it will drop below, say, 0.14.

Table 2 shows that for case B also no eigenvalue approaches zero as h is decreased and thus the approximation is stable. Indeed, for all meshes β_h is already within 3% of the converged value of 0.0781. Since the stabilized

and mini-element formulations are known to be equivalent, the slower convergence of β_h with h for case A as compared to case B is striking. One possible explanation could be that the choice of the stabilization parameter $\tau_K = h^2/4\mu$ is not the optimal one in terms of accuracy, but we have not investigated this further.

It is also worth to inspect the eigenmodes. We show in Fig. 5 the corresponding velocity contours for the stabilized discretization (case A). No evidence of spurious modes is observed. Note also that the eigenmodes 2 and 3 are the same (up to a rotation) and actually the eigenvalues λ_2 and λ_3 converge to the same value as the mesh is refined (as seen in table 1), i.e., this is an eigenvalue of multiplicity two.

On the other hand, when the stabilization is removed *throughout the mesh* the spurious modes clearly show up, as observed in figure 6 where the first eigenmode is shown. This was obtained using Q_h^1 with V_h^1 and standard Galerkin formulation, a combination which is known to be unstable. Note the typical checkerboard pattern in the pressure field (left) and in the velocity magnitude contours (right). Table 3 shows the number of numerically zero eigenvalues (spurious modes) found for the different meshes. We consider an eigenvalue as being numerically zero when its value is smaller than the numerical error of the procedure used to compute it. The results show a roughly logarithmic behavior of the number of spurious modes as function of h.

Numerical computations of the eigenvalue inf–sup problem were also performed in 3D, as described before. The same numerical eigenvalue computation routines were used, resulting in the eigenvalues shown in Tables 4 and 5

Table 3: Number of spurious modes when the stabilization is completely removed.

h	# spurious modes
h_0	1
$h_0/2$	3
$h_0/4$	3
$h_0/8$	3
$h_0/16$	4
$h_0/32$	≥ 6

Table 4: First numerically computed eigenvalues for case A, in 3D.

h	λ_1	λ_2	λ_3	λ_4
h_0	0.10119	0.10165	0.10262	0.10762
$h_0/2$	0.09310	0.09314	0.09324	0.09544
$h_0/4$	0.08913	0.08914	0.08918	0.09040

for cases A and B, respectively. These results display a very similar behavior as in the 2D case. For the stabilized discretization (case A), a reduction in the first eigenvalue is observed, but it is far from tending to zero under mesh refinement. In fact, it only reduced to about 88% of its initial value, in a mesh with approximately 64 times more elements. For the mini-element discretization (case B) we obtained a convergence of the first eigenvalue to a value of about 0.0266 (see Table 5), with the same meshes as in case A.

In summary, there is strong evidence that β_h is bounded away from zero for both Case A and Case B, from which one can conclude that these discretizations involving pressure space Q_h^Γ are indeed convergent. Since in both

Table 5: First numerically computed eigenvalues for case B, in 3D.

h	λ_1	λ_2	λ_3	λ_4
h_0	0.02272	0.02352	0.02363	0.02468
$h_0/2$	0.02691	0.02699	0.02699	0.02703
$h_0/4$	0.02661	0.02681	0.02682	0.02682

cases the *weakened* versions of the stabilized and mini–element formulations were used, it is clear that the same can be said of the *standard* versions, which are necessarily more stable. This is why the eigenvalues of the standard versions have been omitted. Given its stable behavior and its better approximation properties for discontinuous pressures, the space Q_h^Γ compares favourably to the P_1 space for flows with surface tension.

5.2. Stability assessment of $Q_h^{d\Gamma}$ (Cases C and D)

Considering now the modified pressure space $Q_h^{d\Gamma}$ in the discretizations provided by case C and case D, we performed the same calculations as before. Although this space was specifically designed for allowing the enrichment unknowns to be statically condensed, we do not apply condensation here because it would lead turn (43) into a non-linear eigenvalue problem. Hence, for the purposes of stability analysis, we will keep the enrichment unknown and solve problem (eq. 43) as done for cases A and B.

Remark. To see that static condensation leads to a non-linear eigenvalue problem, consider a problem of the form $Au = \lambda u$, where $u = (u_n, u_b)^T$, and we wish to perform a static condensation of the values u_b, resolving the eigenvalues for the resulting condensed matrix and eigenvectors u_n. In that

Table 6: First numerically computed eigenvalues for case C, in 2D.

h	λ_1	λ_2	λ_3	λ_4
h_0	0.14393	0.14458	0.14589	0.18284
$h_0/2$	0.12942	0.13034	0.13087	0.14687
$h_0/4$	0.12343	0.12408	0.12423	0.13367
$h_0/8$	0.11955	0.12002	0.12004	0.12616
$h_0/16$	0.11679	0.11713	0.11713	0.12130
$h_0/32$	0.11483	0.11508	0.11508	0.11806

case,

$$\begin{bmatrix} A_{nn} & A_{nb} \\ A_{bn} & A_{bb} \end{bmatrix} \begin{bmatrix} u_n \\ u_b \end{bmatrix} = \lambda \begin{bmatrix} u_n \\ u_b \end{bmatrix}$$

resulting in

$$\begin{aligned} & A_{nn}\ u_n + A_{nb}\ u_b = \lambda u_n \\ & A_{bn}\ u_n + A_{bb}\ u_b = \lambda u_b \quad \Rightarrow \quad u_b = -(A_{bb} - \lambda \mathbb{I})^{-1}\ A_{bn}\ u_n \end{aligned}$$

and therefore, eliminating u_b, we obtain the eigenproblem

$$\left[A_{nn} - A_{nb}(A_{bb} - \lambda \mathbb{I})^{-1} A_{bn}\right] u_n = \lambda u_n$$

which turns out to be non-linear in λ.

With the same sets of meshes used for cases A and B, the eigenvalues obtained for case C are shown in Tables 6 and 8. The results show strong evidence of the formulation being stable both in 2D and in 3D, confirming what is suggested by the numerical simulations [8]. The space $Q_h^{d\Gamma}$ introduces new unknowns, but since they are statically condensed in simulation codes

Table 7: First numerically computed eigenvalues for case D, in 2D.

h	λ_1	λ_2	λ_3	λ_4
h_0	0.018504	0.022161	0.029465	0.031249
$h_0/2$	0.016267	0.017295	0.021616	0.023510
$h_0/4$	0.009519	0.013267	0.015001	0.017157
$h_0/8$	0.004816	0.005746	0.011841	0.014239
$h_0/16$	0.003413	0.003651	0.006639	0.008651
$h_0/32$	0.001170	0.002001	0.003470	0.004456

Table 8: First numerically computed eigenvalues for case C, in 3D.

h	λ_1	λ_2	λ_3	λ_4
h_0	0.10161	0.10213	0.10321	0.10792
$h_0/2$	0.09312	0.09317	0.09327	0.09327
$h_0/4$	0.08914	0.08915	0.08918	0.09040

the implementation is as easy as that of the P_1 or Q_h^Γ, with one "visible" unknown per mesh node and nothing further. Given its better approximation properties for pressure fields with discontinuous gradients, and given that stability has been shown to hold, $Q_h^{d\Gamma}$ stands as a favourable alternative to the P_1 space for free-surface flows under gravity.

Turning now to case D, let us begin by saying that this formulation is of no practical interest and is only considered here for academic purposes. In fact, the *weakened* stabilization adopted has no pressure–pressure coupling at the elements cut by Γ, precluding the static condensation of the enrichment unknowns which is one of the main attractive features of $Q_h^{d\Gamma}$. Unlike simula-

tion codes, our eigenvalue solver does not condense any unknowns and thus we can evaluate β_h for case D with ease. The purpose of including this case is immediately understood when looking at the obtained eigenvalues, listed in Table 7. Though no eigenvalue is a numerical zero, all four reported in the table decrease *significantly* as the mesh is refined. The inf–sup constant β_h (i.e., $|\lambda_1|$) starts with a value of 1.85×10^{-2} for the coarsest mesh. After five refinements, it has already fallen to 1.17×10^{-3}. By least–squares–fitting β_h as a function of h from the computed values one gets $\beta_h \simeq 0.1\, h^{0.8}$, clearly indicating that $\beta_h \to 0$ with a power of h that is comparable to that of the (order h) interpolation error. This case exemplifies a formulation that, although it has no spurious modes (the matrix for any given mesh is invertible), the inf–sup constant tends to zero in a way that will make it converge suboptimally (if at all) to the exact solution. Arguably, the widely different behavior of case D (diagnosed as unstable) from cases A to C (diagnosed as stable) endowes our numerical assessment methodology with some credibility as diagnostic tool.

5.3. Generalizing the stability assessment methodology

The results presented in the previous subsections can be summarized, in terms of numerical stability, as follows:

a) The space Q_h^Γ behaves essentially as the space P_1. Coupled with V_h^1 for velocity it is stable under stabilization, while coupled with V_h^{mini} it is stable with the Galerkin formulation. For this space, as for the P_1, velocity enrichment with bubble functions is roughly equivalent to elementwise residual stabilization. This is concluded from Cases A and B above.

b) Further, also from cases A and B, it is observed that if stabilization (or, equivalently, the bubble-enrichment of the velocity) is inhibited in the band of elements crossed by Γ, stability is preserved. The inf-sup constant "does not care" that there is a band of weakened elements in the mesh. Though this is perhaps expected, it is not completely obvious and caught our attention. Later on in this section we apply the numerical assessment methodology to show that this behavior has nothing to do with the discontinuity at Γ of Q_h^Γ, since the possibility of "weakening" an arbitrary band of elements also takes place for the P_1 space Q_h^1.

c) The results of Case C (Tables 6 and 8) tell us that the enriched space $Q_h^{d\Gamma}$, though larger that Q_h^1, still can be properly controled by the velocity space V_h^1 in the standard stabilized formulation and thus that the method proposed by Coppola-Owen and Codina is indeed optimally convergent. Qualitatively, the behavior of λ_1 with h is very similar to that of Case A. Stability has also been confirmed to hold for the pair $Q_h^{d\Gamma} - V_h^{\text{mini}}$ for the Galerkin formulation, in computations not reported here for brevity, confirming the behavioral equivalence of the stabilized and mini formulations once more.

d) In case D, on the other hand, two sources of instability have been introduced in the band of elements containing Γ with respect to the standard stabilized P_1/P_1 method: (i) The stabilization has been removed, and (ii) the pressure space has been enriched with bubble functions. Not surprisingly, the resulting method has symptoms of instability,

and these symptoms are easily identifiable from the eigenvalue analysis adopted.

One objection that can be raised against the conclusions drawn above is that the interface shapes tested were only two, a circle and a sphere. To overcome this limitation in the assessment, we adopted the strategy of solving the eigenproblem (43) on a fixed mesh for *ten thousand random configurations of* Γ_h.

In 2D we consider the unstructured mesh of 13312 elements corresponding to $h = 0.025$. To generate the random Γ_h for each test, we consider polynomials in x and y of the form

$$\Phi(x, y) = r_1 x + r_2 y + r_3 xy + r_4 x^2 + r_5 y^2 + 10\ r_6 x^3 + 10\ r_7 y^3 \tag{59}$$

where the coefficients r_i, $i = 1, \ldots, 7$ are random numbers generated in the interval $[-1, 1]$. This function is interpolated to obtain Φ_h, and then Γ_h is obtained as the zero level set of Φ_h as already explained (equation 55). Since Φ is zero at $(0, 0)$, $\Gamma_h \cap \Omega$ is not empty. Some examples of the random Γ_h can be seen in Fig. 7. In Fig. 10 histograms of the angle formed between at interface/edges intersections, as well as of the volume fraction distribution of the cut elements, are displayed. They show that the random shapes assure a great variety of element/interface intersections. Though obviously not all possible interface configurations can be explored, we believe that the set of tested configurations is large enough to draw convincing conclusions.

The computations were performed for several cases, of which we report here only two:

- **Case E:** Q_h^1–$V_h^{\text{mini},0}$ (i.e., *weakened mini–element formulation*);

- **Case F:** $Q_h^{d\Gamma}$ and V_h^1 with *weakened* stabiliza tion (i.e.; identical to case D);

The rationale for this choice is as follows: Case E corresponds to a formulation essentially equivalent to Case B (since as said Q_h^{Γ} behaves as Q_h^1), which for the circle was found to be stable. In turn, as already discussed, Case B behaves essentially as Case A, as expected from the equivalence between the mini–element and the stabilized formulations. It was confirmed that these equivalences (case A $\equiv$ case B $\equiv$ case E), already reported for the circle and the sphere, also hold for the random–generated interfaces, and thus only one of them is reported. The specific choice of reporting Case E is because it corresponds to *the plain–vanilla* P_1^+/P_1 *mini–element formulation, from which the bubbles have been removed in a random band of elements.* Given the wide spread of the mini–element, not restricted to multiphase flow problems, it was deemed more interesting to report the statistical results of Case E instead of A or B above. Case C is also not reported in detail because the statistical treatment also confirms the conclusions drawn on the basis of the circle/sphere results.

The results for case E can be seen in Fig. 8. In this figure, we display the histograms of the first (left) and second (right) eigenvalues. Both eigenvalues in all the random realizations are clustered between 0.05 and 0.08, with no evidence that the distribution has a tail that may reach the zero value. This behavior is also observed for the formulations of cases A, B and C and is deemed as evidence of *stability*. The same behavior is also observed for the equal–order P_1/P_1 formulation, with either standard or weakened stabilization.

Notice, on the other hand, that Case F is exactly the same as Case D above, which was diagnosed as unstable. This case is reported for comparison purposes, since it lets us show the difference in behavior of stable and unstable formulations when subjected to statistical stability assessment.

For case F, the corresponding histograms are displayed in Fig. 9. The eigenvalues are not only smaller, but their distribution seems to reach the zero value with positive probability density. The minimum eigenvalue found, over all random interfaces, was $\beta_h = |\lambda_1| = 1.24 \times 10^{-4}$, more than one hundred times smaller than the maximum β_h found, which was 0.02. This behavior, completely different from that of case E, is diagnosed as *unstable*, confirming our conclusions of case D.

Remark. Depending on the refinement of the mesh and on the morphology of Γ_h, the inf–sup constant β_h could be zero for some realization. These are isolated occurrences that happen if, *and only if*, a mesh node is completely surrounded by elements crossed by Γ_h. By construction, the weakened stabilization assigns no stabilization at all to the equation corresponding to the surrounded node, resulting in a null eigenvalue. The same happens to the weakened mini–element formulation when the bubbles are removed in all elements that share any given node. This pathology may in general be avoided by increasing the mesh resolution. Figure 11 displays a case in which β_h is zero for the two coarsest meshes. After the third refinement, the mesh represents the surface well enough for pathologic nodes not to appear. In the histograms reported here any case with a node completely surrounded by weakened elements is therefore disregarded.

Concerning statistical assessments in 3D, the solution of a generalized eigenvalue problem turns out to be very CPU demanding, given the number of unknowns for a moderate size tetrahedral mesh. This makes a thorough statistical analysis too costly in terms of CPU time. We illustrate here some 3D calculations generated by random configurations of the interface. Let us consider as before

$$\Phi(x,y,z) = r_1 x + r_2 y + r_3 z + r_4 xy + r_5 xz + r_6 yz + r_7 x^2 + r_8 y^2 + r_9 z^2 + 10\, r_{10} x^3 + 10\, r_{11} y^3 + 10\, r_{12} z^3 \quad (60)$$

where r_i, $i = 1, \ldots, 12$ are random numbers in $[-1, 1]$. By the same procedure as in 2D, we generated random Γ_h for the eigenvalue analysis. Examples of the generated surfaces can be seen in Fig. 12. For each example, the inf-sup constant β_h corresponding to case E, computed with a mesh of 309500 tetrahedra, is also shown. Notice that the eigenvalues are all very similar though the surfaces are widely different. The eigenvalues are tightly clustered around a mean value of about 0.024, which in turn is quite close to that obtained for the sphere in case B. Of course the number of random combinations is limited to draw robust conclusions, but the evidence suggests that stability also holds in 3D. This is consistent with the success of 3D simulations carried out for a number of applications with the weakened stabilized formulation [9, 22, 18].

6. Conclusions

In this work, we have presented numerical evidence of convergence of modified pressure spaces usually employed in multi-fluid flow simulations. No

mathematical stability analysis or proof of convergence for such discretizations is yet available. The numerical stability assessment carried out here follows the work of Malkus [15], computing the inf–sup constant β_h by solving a generalized eigenvalue problem.

The spaces analyzed correspond to those originally proposed by Ausas et al [9] and by Coppola–Owen & Codina [8]. The first one is designed to capture discontinuities in the exact solution by locally modifying the P_1 shape functions. The second one enriches the P_1 pressure space with a condensable bubble in order to improve the representation of discontinuities in the exact pressure gradient. By analyzing the computed inf–sup constants, it was shown that both of these spaces, and their corresponding formulations, are indeed stable and thus convergent.

Further, we have investigated the effect of weakening the stability of an otherwise stable formulation in an arbitrary band of elements, such as those elements cut by an arbitrary interface Γ. This was accomplished by setting the stability coefficient to zero in those elements, for stabilized formulations, and by removing the velocity bubble functions in those elements, for mini–element formulations. The investigation showed that, for all the studied formulations of practical interest (including the stabilized equal–order P_1/P_1 element and the plain vanilla P_1^+/P_1 mini–element) stability, and thus optimal–order convergence, are *not* affected. Users of equal–order (or mini–element) formulations can quite safely remove the stabilization (or, respectively, the velocity bubbles) on an arbitrary band of elements without expecting any misbehavior of the flow solver, provided, as discussed, that this band does not have any mesh node internal to it.

Acknowledgments

The authors thank Prof. Enzo Dari and the anonymous reviewers for useful suggestions and hints. Support from Brazilian funding agencies FAPESP and CNPq are gratefully acknowledged. This research was carried out in the framework of INCT-MACC, Ministério de Ciência e Tecnologia, Brazil.

References

[1] S. Ganesan, G. Matthies, and L. Tobiska. On spurious velocities in incompressible flow problems with interfaces. *Comput. Methods Appl. Mech. Engrg.*, 196(7):1193–1202, 2007.

[2] R. Rangarajan and A. Lew. Universal meshes: A new paradigm for computing with nonconforming triangulations. Submitted. ARXIV: arxiv.org/abs/1201.4903.

[3] S. Gross and A. Reusken. Finite element discretization error analysis of a surface tension force in two-phase incompressible flows. *SIAM J. Numer. Anal.*, 45:1679–1700, 2007.

[4] S. Gross and A. Reusken. An extended pressure finite element space for two-phase incompressible flows with surface tension. *J. Comput. Phys.*, 224:40–58, 2007.

[5] A. Reusken. Analysis of an extended pressure finite element space for two–phase incompressible flows. *Comput. Visual. Sci.*, 11:293–305, 2008.

[6] T. Belytschko, N. Moës, S. Usui, and C. Parimi. Arbitrary discontinuities in finite elements. *Int. J. Numer. Meth. Engng.*, 50:993–1013, 2001.

[7] P.D. Minev, T. Chen, and K. Nandakumar. A finite element technique for multifluid incompressible flow using Eulerian grids. *J. Comput. Phys.*, 187:225–273, 2003.

[8] A.H. Coppola-Owen and R. Codina. Improving Eulerian two-phase flow finite element approximation with discontinuous gradient pressure shape functions. *Int. J. Num. Meth. Fluids*, 49:1287–1304, 2005.

[9] R.F. Ausas, F.S. Sousa, and G.C. Buscaglia. An improved finite element space for discontinuous pressures. *Comput. Methods Appl. Mech. Engrg.*, 199:1019–1031, 2010.

[10] D. Arnold, F. Brezzi, and M. Fortin. A stable finite element for the Stokes equations. *Calcolo*, 21:337–344, 1984.

[11] T.J.R. Hughes, L. Franca, and M. Balestra. A new finite element formulation for computational fluid dynamics: V. Circumventing the Babuška-Brezzi condition. A stable Petrov-Galerkin formulation of the Stokes problem accommodating equal-order interpolations. *Comput. Methods Appl. Mech. Engrg.*, 59:85–99, 1986.

[12] L. Franca and T.J.R. Hughes. Two classes of mixed finite element methods. *Comput. Methods Appl. Mech. Engrg.*, 69:89–129, 1988.

[13] G.C. Buscaglia and A. Agouzal. Interpolation estimate for a finite-element space with embedded discontinuities. *IMA J. Numer. Anal.*, 32:672–686, 2011. DOI 10.1093/imanum/drq045.

[14] R. Stenberg. A technique for analysing finite element methods for viscous incompressible flow. *Int. J. Num. Meth. in Fluids*, 11:935–948, 1990.

[15] D.S. Malkus. Eigenproblems associated with the discrete LBB condition for incompressible finite elements. *Int. J. Engng. Sci.*, 19:1299–1310, 1981.

[16] A. Huerta, Y. Vidal, and P. Villon. Pseudo-divergence-free element free Galerkin method for incompressible fluid flow. *Comput. Methods Appl. Mech. Engrg.*, 193(12-14):1119–1136, 2004.

[17] E. Bänsch. Finite element discretization of the Navier–Stokes equations with a free capillary surface. *Numer. Math.*, 88:203–235, 2001.

[18] G. Buscaglia and R. Ausas. Variational formulations for surface tension, capillarity and wetting. *Comput. Methods Appl. Mech. Engrg.*, 200:3011–3025, 2011.

[19] A. Ern and J-L. Guermond. *Theory and Practice of Finite Elements*. Springer, 2004.

[20] I. Babuška. The finite element method with Lagrangian multipliers. *Numer. Math.*, 20:179–192, 1973.

[21] F. Brezzi. On the existence, uniqueness and approximation of saddle–point problems arising from Lagrange multipliers. *RAIRO Anal. Numér.*, 8:129–151, 1974.

[22] F.S. Sousa, R.F. Ausas, and G.C. Buscaglia. Improved interpolants for discontinuous pressures. *Mecánica Computacional*, 28:1131–1148, 2009.

[23] V. Fernández, J.E. Román, and V. Vidal. SLEPc: Scalable Library for Eigenvalue Problem computations. *Lecture Notes in Computer Science*, 2565:377–391, 2003.

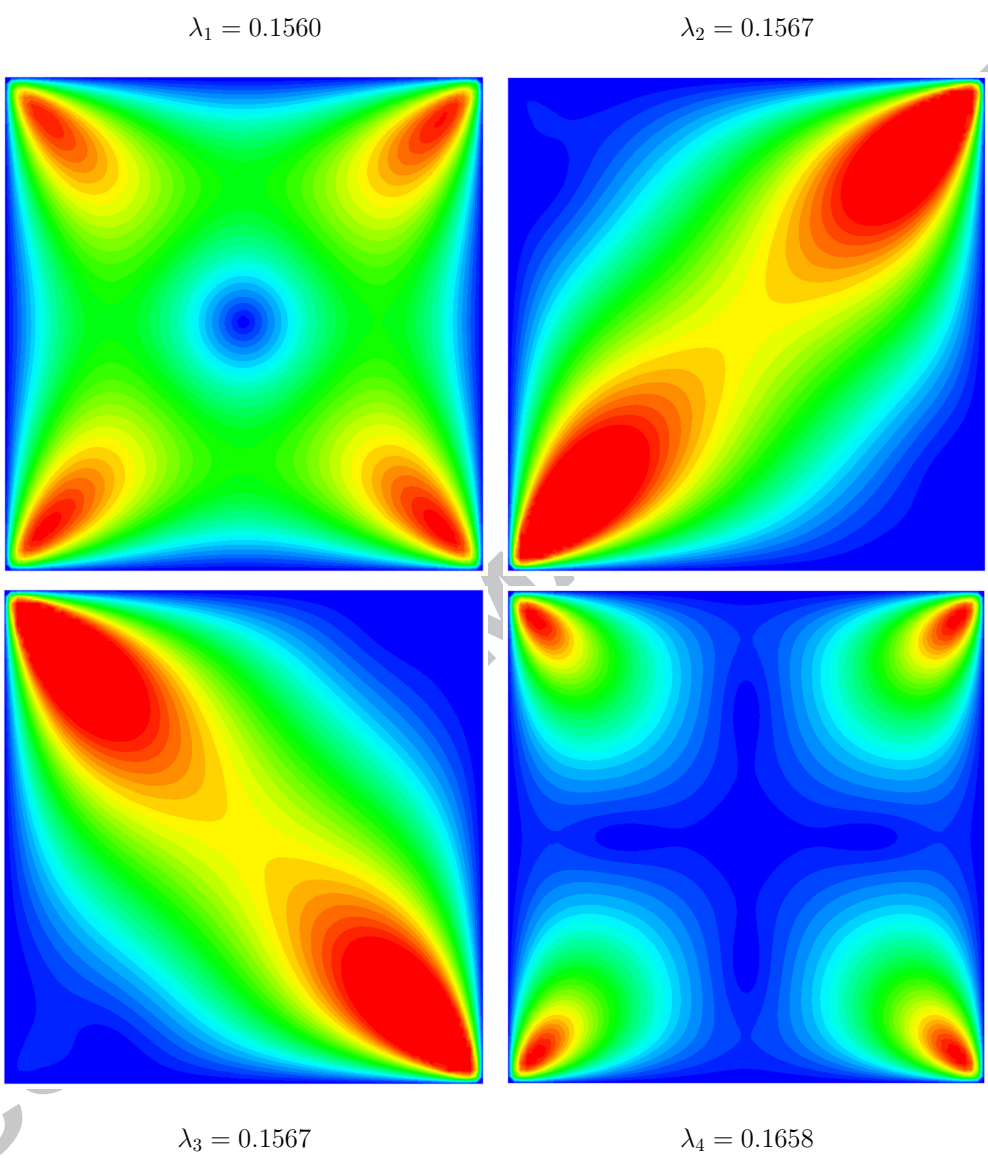

Figure 5: Velocity magnitude for the first eigenmodes of problem (43) obtained for Case A in 2D. Results corresponds to the third level of refinement ($h_0/8$).

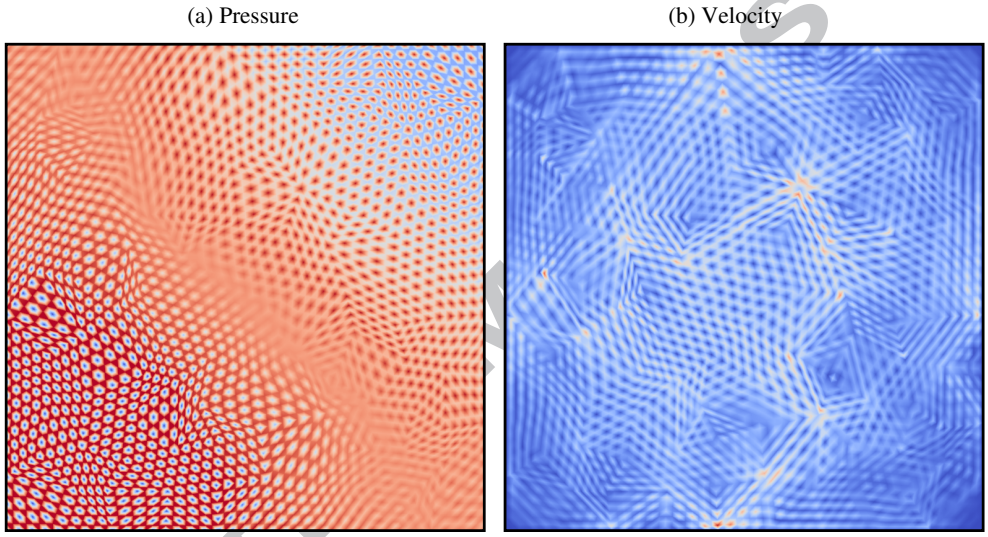

Figure 6: Spurious modes appearing when the stabilization is completely removed. Shown are contours of pressure (a) and of velocity magnitude (b) for the first eigenmode, corresponding to the third level of refinement ($h_0/8$).

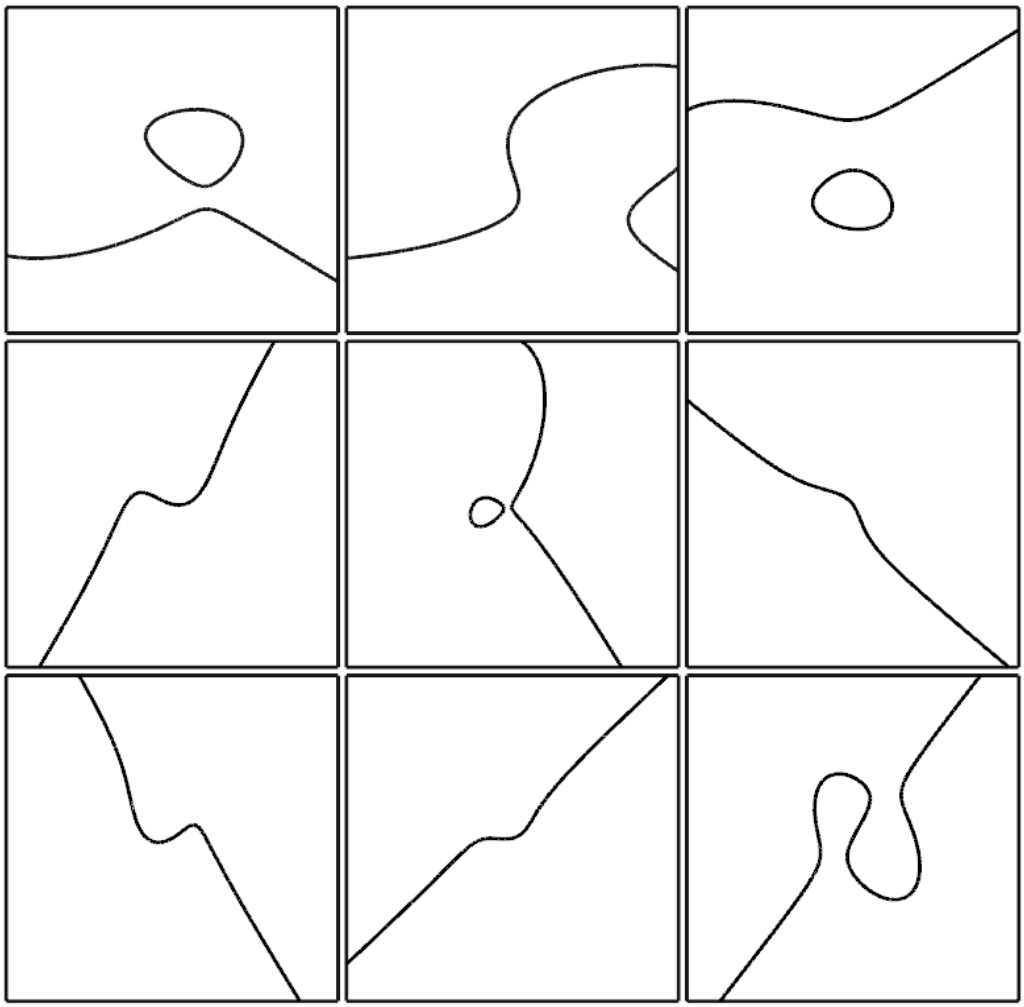

Figure 7: Examples of random interfaces generated for the statistical assessment in 2D.

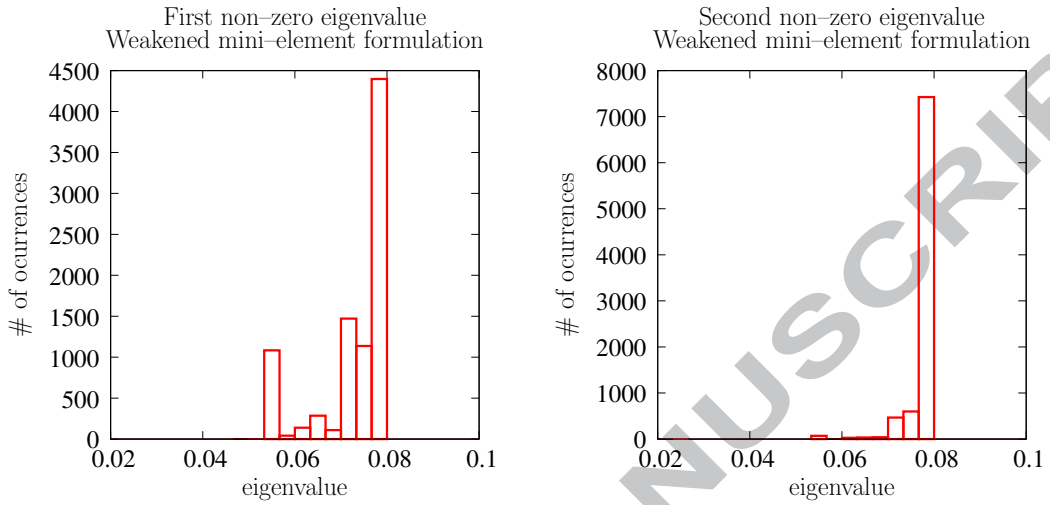

Figure 8: Histograms for the first two computed eigenvalues for case E in 2D.

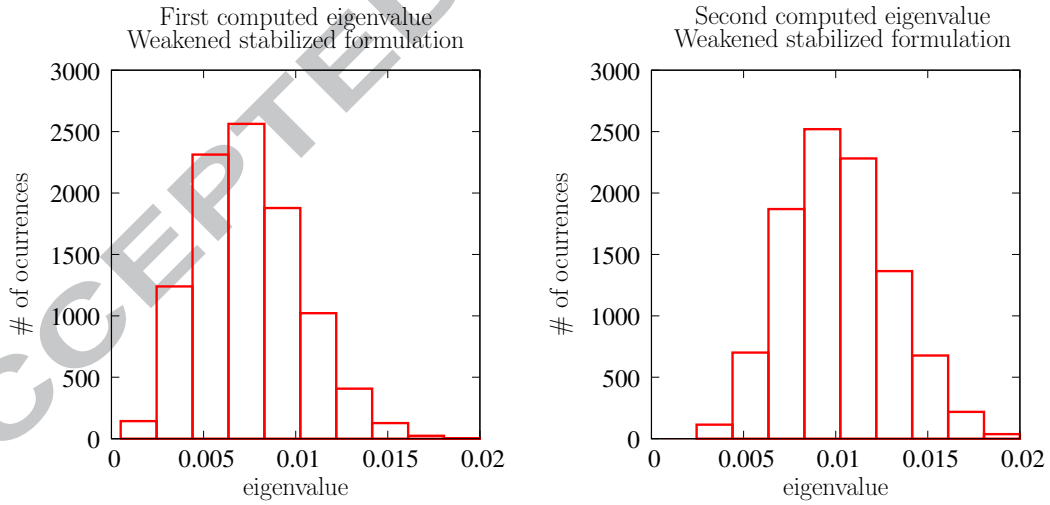

Figure 9: Histograms for the first two computed eigenvalues for case F in 2D.

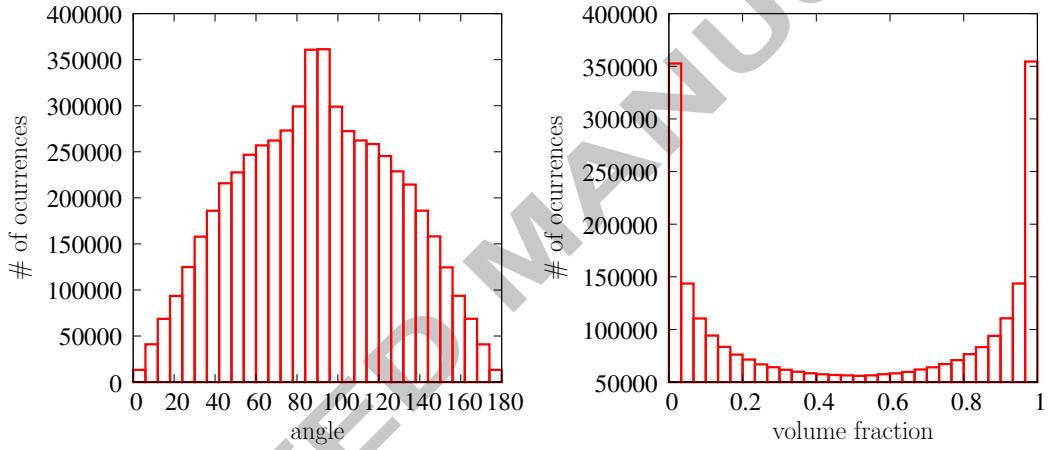

Figure 10: Histograms for the angle between interface and edges at intersections (left) and for the element's volume fraction cut by the interface (right), for case F in 2D.

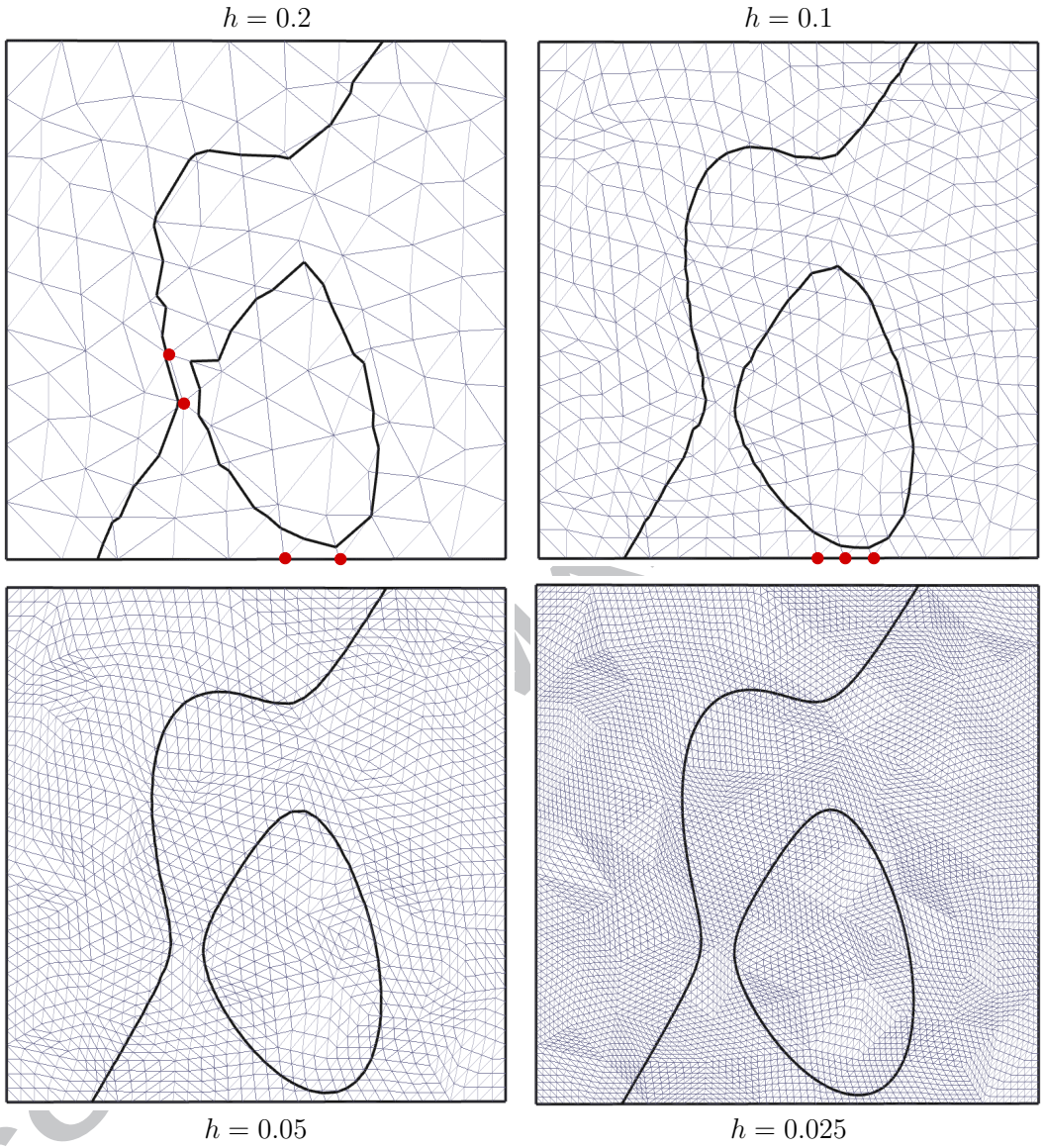

Figure 11: Refinement study of a random interface that for the coarsest mesh has pathologic nodes completely surrounded by elements cut by Γ_h. Red dots indicate the pathologic nodes, if any, in each mesh. The corresponding inf–sup constant for the formulation of case E is as a consequence zero for the two coarser meshes (top row). The two finer meshes (bottom row), having no pathologic nodes, yield $\beta_h > 0$.

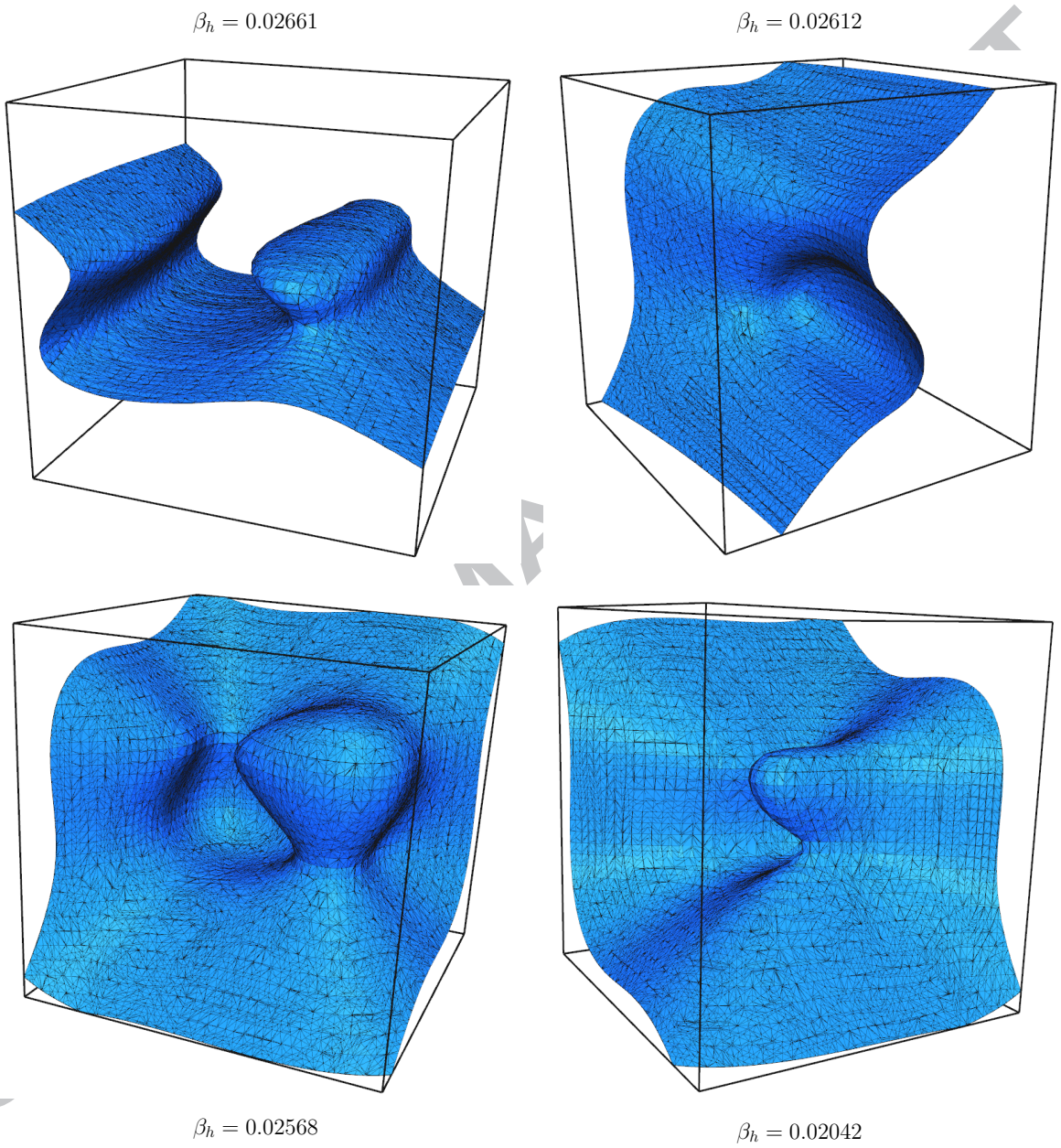

Figure 12: Examples of random interfaces generated for the stability analysis in 3D. The computed values of β_h are also reported for each case.

Highlights:

- Inf-sup constants of several formulations are evaluated by solving generalized eigenproblems;
- We prove the stability of two interface-discontinuous FE spaces designed for multiphase flows;
- We prove that the stabilized P1/P1 formulation does not become unstable if stabilization is removed in a band of elements;
- We prove that the mini-element formulation does not become unstable if the velocity bubbles are removed in a band of elements;